Eskers in a complete, wet-based glacial system in the Phlegra Montes region, Mars

Journal Item

Eskers in a complete, wet-based glacial system in the Phlegra Montes region, Mars

Colman Gallagher[1,2], Matthew Balme[3,4]

[1]UCD School of Geography, University College Dublin, Belfield, Dublin 4, Ireland

colman.gallagher@ucd.ie

[2]UCD Earth Institute, University College Dublin, Belfield, Dublin 4, Ireland

[3]Dept. of Physical Sciences, Open University, Walton Hall, Milton Keynes MK7 6AA, UK

[4]Planetary Science Institute Tucson, 1700 E. Fort Lowell, Suite 106, Tucson, AZ 85719, United States

Abstract

Although glacial landsystems produced under warm/wet based conditions are very common on Earth,even here,observations of subglacial landforms such as eskers emerging from extant glaciers are rare. This paper describes a system of sinuous ridges emerging from the *in situ* but now degraded piedmont terminus of a Late Amazonian-aged (~150 Ma) glacier-like form in the southern Phlegra Montes region of Mars. We believe this to be the first identification of martian eskers that can be directly linked to their parent glacier. Together with their contextual landform assemblage, the eskers are indicative of significant glacial meltwater production and subglacial routing. However, although the eskers are evidence of a wet-based regime, the confinement of the glacial system to a well-defined, regionally significant graben, and the absence of eskers elsewhere in the region, is interpreted as evidence of sub-glacial melting as a response to locally enhanced geothermal heat flux rather than climate-induced warming. These observations offer important new insights to the forcing of glacial dynamic and melting behaviour on Mars by factors other than climate.

Keywords: Mars; glacier; eskers; wet base; geothermal control.

1. Introduction

The Phlegra Montes upland extendsNNE-SSW over 1000 km, between 30 N and 52 Non Mars (Fig. 1). Southern Phlegra Montes, 560 km east of Hecates Tholus on the Elysium rise,is90 to 180 km wide, overlooking the Elysium Rise to the west and sloping towards aflanking N-S trending piedmontbasin to theeast. Theupland relief is dominated by rounded peaks,intervening valleysand basins, some partially occupied by icyfills (Safaeinili et al., 2009; Dickson et al., 2010). The valley fills are longitudinally lineated (‘lineated valley fills’ or LVF; Squyres, 1979),like the basin fills exhibiting ridges, troughs and lobes. These morphologies, suggesting flow over or around obstaclesinresponse to changes in underlying slope, are typical of ‘viscous flow features’ (VFF; Milliken et al., 2003). These characteristics, together with associated erosional (mainly upland) and depositional (includingpiedmont)landforms such as moraine-like ridges are regarded as evidence that VFF andLVF are glaciers, or glacier-like forms (GLF; Souness et al., 2012; Hubbard et al., 2014), formerly thicker and more extensive. The crater retention age of these landforms indicates they formedover the past ~600 Ma (Kress et al., 2010; Fassett et al., 2014), most recentlyin the Late Amazonian(Milliken et al., 2003; Hubbard et al., 2011; Souness et al., 2012; Hubbard et al., 2014). In common with other low plains bounding uplands, the Phlegra Montes piedmont is characterized by lobate debris aprons (LDA), accumulations of ice mantled by lithic debris (Kochel and Peake, 1984; Holt et al.,2008; Parsons et al., 2011; Fastook et al., 2014).

Fig. 1 here.

The majority of observational glaciological and landform evidence shows that extant martian glaciers/GLF are cold/dry based (Hubbard et al., 2011; Hubbard et al., 2014)and (were) dynamic by virtue of creep (Milliken et al., 2003; Parsons et al., 2011); the landform evidence for relict glacial process-environments suggests this has been characteristic of Amazonian glaciation. Observations of landforms in contextually consistent landsystems diagnostic of warm/wet based glacial regimes on Mars, especially eskers,are rare in comparison to the widespread presence of glaciers.Kargeland Strom (1991), however,were confident that many sinuous, often branching, ridges on Mars are eskers that, as on Earth, display a wide size range and ridge-network variety, ranging from single to branching to arborescent and braided. More recently, several researchers have concluded that sinuous ridge systems in Dorsa Argentea (Head, 2000) and Argyre Planitia(Banks et al., 2009; Bernhardt et al., 2013) are eskers, the latter reflecting subglacial routing of pressurized meltwater, generated both supraglacially and englacially, through Rothlisberger (R) channels cut upwards into extensive Hesperian glacial ice. On Earth, landsystems produced under warm/wet based conditions, including organized englacial to subglacial meltwater routing and sediment flux,are very common, dominating the landscapes of many deglaciated areas. However, observations of subglacial landforms in a state of emergence from degrading but extant glacial ice are rare, even on Earth, and previously un-reported on Mars. This paper describes a system of sinuous ridges emerging from the degraded piedmont terminus of a LVF/GLFin the southern Phlegra Montes region.Based on analysis of the landsystem as a whole, the conclusion is that these landforms are eskers emerging from a decayed glacial margin. Together with theircontextual landform assemblage, the eskers are indicative of significant glacial meltwater production and subglacial routing – by definition evidence of a wet-based regime. Whether they are indicative of aclimatically-determined warm-based regime is discussed, and alternatives considered.

2. Approach

2.1 Data

Covering the study area,a mosaic of seven,6 m/pixel, georeferenced ConTeXt camera (CTX, Malin et al., 2007) images(Appendix 1 and 2) was constructed using ArcGIS. Other data included a High Resolution Stereo Camera (HRSC; Neukumand Jaumann, 2004) image and its associated Digital Elevation Model (DEM), and gridded Mars Orbiter Laser Altimeter (MOLA; Zuber et al., 1992) topography data. The MOLA data have low spatial resolution (~500m gridding) but high vertical precision (~1m). The HRSC DEM has higher spatial resolution (75m gridding) butvertical precision similar to the spatial resolution of the original image data (i.e. about 12 m).

2.2Determining the age of the system using impact crater size-frequency statistics

Planetary surfaces can be dated using impact crater size-frequency distribution data, although this becomes complicated following resurfacing,surface modification or downwasting (Michael and Neukum, 2010). It is also difficult when considering small areas in which insufficiently large populations of craters have accumulated to provide statistically reliable ages (Warner et al., 2015). Both problems apply to thelandsystem in Phlegra, as the LVF has probably downwasted over time through loss of ice, and the extent of the LVF and associated landforms is only a few 100km^2 in areal extent. To estimate the formation and modification ages of the system, the size-frequency distribution of impact craters was measured for various sub-regions using the ArcGIS add-ons *Cratertools*(Kneissl et al., 2011) and plotted using the tool*CraterStats*(Michael and Neukum, 2010).

The *CraterTools* 3-point method was used to digitise the rims of all visible impact craters. Crater discrimination was complicated by the many rimless circular features on the LVF - most are probably degraded craters but the relationship between their present and original diameter is unclear. We counted all the crater-like circular features, recording their current diameter. Consequently, this crater-count errs towards overestimating the crater retention age of the LVF. However, this is balanced to an unknown degree by the likely loss of many craters from the LVFsurface due to sublimation and flow deformation. Hence, owing to the small count area, the low number of craters counted and surface modifications, the count data for the LVF especially giveonly a first order approximation of the age.

3. Observations: landsystem components.

The main landsystem components (Fig. 2a) are aparallel-sided, trough-like valley, striking WNW-ESE through the far-southern Phlegra Montes upland (Fig.2, Zones 1-2), and a relatively shallow trench extending through the eastern piedmont directly along strikefrom the upland valley(Zones 3-4). The valley is occupied by a diffluent LVF, descending to the western and eastern piedmonts(Fig.2b, Fig 3a).Tributary troughs containing backwasted LVF, which no longer reach their confluence,incise the plateauoverlooking the valley (Fig.3b). The LVF is patterned by lineated,viscous features - the surface expression of glacier-like flow that characterises GLFs (Milliken et al. 2003; Souness et al., 2012). Eastof the LVF, a pitted zone follows thesame topographic trend (Fig. 2, Zone 2).The trenchincisingthe eastern piedmont(Fig. 2, Zones 3 and 4)is occupied by a fill that varies from hummocky and intensely pitted to longitudinally-furrowed. The trench is laterally bounded by higher, pitted piedmont surfacesand terminates at a low-lying, distal basin occupied by a fractured, level fill (Fig. 2, Zone 5).A complex of sinuous ridges is located at the terminus of the trench fill. The piedmont surface close to the upland is mantled by pitted mass-wasting deposits shed from the bounding slopes. The distal piedmont is less intensely pitted but, like those of the proximal piedmont, the pits are themselves internally textured by smaller pits. The upland LVF descending eastward,the piedmont trench-fill(PTF) and its terminal zone sinuous ridges are thefocus of this paper.

Fig. 2 here

3.1 Zone1

The apex of the LVF descending eastward occupies the widest part of the upland valley: ~11 km across (Fig 2). This zone is a flattened dome with a subtle, hummocky surface.The depth of the LVF is unknown. Although there are SHARAD (Seu et al., 2007) RADAR profiles across the system, showing a possible sub-surface reflector, their usefulness iseliminatedby the presence of off-nadir 'clutter'.The LVF narrows downvalley to the east, becoming 7.9 km wide at its present terminus, 15.5 km from the apex. The LVF is not a simple form but consists ofasymmetric lobes converging from the valley sides to its mid-line (Fig. 3a). The LVF surface is longitudinally lineated, with alignments replicating the changing asymmetry of the constituent lobes as the valley widens or narrows.Degraded ring-mold impact craters, thought to indicate impact into near-surface ice (Kress and Head, 2008), and a few fresh cratersoccur on the LVF surface (Fig 3a).Zone 1 terminates at a 900 m-long, back-sloping belt of irregular pits and blocky hummocks spanning the valley, here ~7 km wide (Fig 4a). Individual pits are at most 100 – 300 m wide, hummocks 100 – 250 m, and the entire assemblage stands up to ~80 m higher than the LVF terminus.

Fig 3 here.

3.2 Zone 2

The first pitted band at the foot of the LVF marks the beginning of a 3.3 km-long reach ofvalley fill (Fig 4a) terminating at another cross-valley belt (pit band 2) of 100m-scale pits and hummocks. This belt marks the start of a 6.8 km-long reach of pitted, hummocky fill, bounded by two prominent converging headlands (A and B, Fig. 4a) that define a narrow valley (head at 'P', Fig. 4a). The headlands were formed by the breachingof an originally continuous transverse bedrock ridge at its lowest point ('Q', Fig. 4a). The breach is ~0.8 km wide and ~30 m deep from the level of its shoulders. Although the lateral margins of the Zone 2 hummocky and pitted fill are generally in contact with both valley sides, a small valley extends from the southern limb of the breached ridge for ~4 km into the LVF. This re-entrant (X to Yin Fig. 4a) ischaracterised by longitudinally linked alcoves,up to 1.5 km wide,and a sharply defined sinuousvalley axis.

Fig. 4 here

3.3 Zone 3

Beyond the breached bedrock ridge delimiting Zone 2, for ~30km along the same strike as the upland valley, the eastern piedmont is indented by a 3 – 5.5 km-wide trench containing the PTF. In the proximal eastern piedmont, the trench is laterally bounded by well-defined walls, rising up to 100 m above the intensely pitted, hummocky PTF (Fig.4b) and indented by erosional alcoves, best developed on the north-facing wall (white arrows, Fig. 4b). A suture-like crease, expressing the axial continuation of the ridge-breach in Zone 2, continues into the Zone 3 PTF (black arrows, Fig. 4b). Zone 3 has a shallow eastward-dipping slope, compared with the steep, convex slopes that mark the eastern half of Zone 2 (Fig. 2b).

3.4 Zone 4.

Zone 4 encompasses the PTF traversing the distal eastern piedmont. The transition from Zone 3 is subtle, but distinct, marked by a change in the pattern and albedo of the hummocky pitted fill. The zone has three sub-zones, each showing increasing amounts of connectivity along channel-like systems.

Zone 4a:From the end of Zone 3 for ~4.8 km, the northern and southern PTF margins are dominated by relatively low albedo, convex-up, longitudinally-furrowed, undulating swaths up to ~1 km wide(FN and FS, Fig 5a). Most of the central tract along this PTF reach is disrupted into a curving series ofalternating bulbous steps and depressions. MOLA and HRSC DEM data suggest this tract is ~10m lower than FN and FS. The longitudinally-furrowed swaths,therefore, are flanking platforms bounding the disrupted tract. Both bounding platforms terminate at a poorly-defined, low, curving scarp marking the transition to Zone 4b but which, in the central disrupted tract, cuts 1 km back into Zone 4a. Some longitudinal furrows appear to cross into Zone 4b, whereas the disrupted steps and depressions terminate at, or form, the disrupted scarp. Although at the limits of HRSC vertical resolution, the topographic interpretationsare supported by both MOLA data andthe morphology of the central tract.

Zone 4b: For ~4 km from the end of Zone 4a, the PTF is partly surfaced by the continuation of FN and FS (Fig. 5b), here ~1.5 – 2.5 km-wide. They are separated by longitudinally lineated or pitted PTF, fronting the depressed, disrupted central tract of Zone 4a, and bounded laterally by the piedmont surface. FN extend from the terminal edge of the disrupted Zone 4a surface. FS are higher than FN and descend from Zone 4a onto Zone 4b, bifurcatinginto northern and southern branches (FSn and FSs respectively), which together surround a ~5 kmdiametercircular mass of intensely pitted (including internal subsidiary pits), hummocky material. FSncross-laps FN,passes under the northwestern limb of the circular massbut reappearsat itsnortheastern limb. FSs curvestowards the southern margin of the trench, around the perimeter of the circular mass,re-joiningand cross-cutting FN. Overlying and infilling parts of FSs are discontinuous patches of low-albedo material. Where FS re-joins FN (Fig.5b, small arrows),this material partly infills furrows in the northern region. Given the cross-cutting relationship (southern furrows postdate the northern), this could indicate that the low-albedo material was transported along the FS furrow system and backfilled FN(Fig. 5b).

Fig. 5 here

Zone 4c: The Zone 4b furrows terminate at a scoop-shaped embayment cutting into the PTF(Fig.6a). Based on shadows, the exposure along the sloping backwall appears tiered,suggesting that the furrowed material islayered. The embayment is bisected by an axial trough, and narrow, sinuous ridges are present on its floor(Figs.6a and 6b).In the proximal end of this ridge system, two parallel ridges (RpN and RpS) are partially exposed.Trending WNW-ESE, they are initially continuous for~0.5 – 2 km, and are ~70 m wide and 150 – 300 m apart.After about 3 km, the two ridges diverge and develop subtly different morphologies.RpS has a simpler form thanRpN, being sharp crested and nearly continuous, formed of only four or so sections, over a path length of ~10 km. RpN,though, becomes discontinuous and more complex, bifurcating to forma medial pair of ridges consisting of offset straight segments, 80 –

300 m long, forming a disjointed curve, with up to 140 m between segments. The terminus of one branch of the birfurcated RpN ridge system is obscured by rough terrain, but the southern branch isvisible, although discontinuous, until iteither becomes confluent with, or is cross-lapped by, theend of RpS. Beyond this confluence, the two ridge systems form a single, discontinuous, ~6 km long, segmented complex (Rd) of short, broad-crested, lozenge-like ridges, each a few hundred meters or lessin length and separated longitudinally by >50 m. Some segments appear to cross-lap others, some to run beside adjacent segments.

Fig 6 here

3.5. Zone 5

East of the Zone 4c ridges, the terrain drops slightly into a flat elongatedbasin, 250 km long (north-south) and up to 70 km wide (Figs 2 and 7a). The margin of the basin fill has an extremely narrow elevation range l (Fig 7b) but its surface is subtly fractured in places, gently hummocky andmorphologically distinct from Zone 4c and the bounding piedmont zones. The basin fill surface contains large numbers of impact craters but no ring-mold forms (although many have apparently smooth, perhaps “icy”, fills)as present on the LVF. Lobate debrisaprons marginally transgressing the fill in the north of the basin (centred onX in Fig. 7b)contain only a few impact craters, some being ring-mold forms.

3.6. Age of the system – impact crater size-frequency statistics

To estimate the formation and modification ages of Zone 1 and 5, the size-frequency distribution of impact craters was measured on the 180 km^2 surface of the LVF/GLF east of the apex and across the entire 6100 km^2 of Zone 5, defined by its mapped marginal contact (Fig 7b).In Zone 5, using HRSC nadir image h1423_0001, only craters >20 pixels across (250m) were reliably identified. For Zone 1, less noisy CTX images were used (Appendix 3) and craters larger than about 15 pixels across (90m) were recorded.

Computing the crater retention age in *CraterStats,* using the Ivanov (2001) Mars production function and the Hartmann and Neukum(2001) chronology, the crater diameter range best matching an isochron for Zone 1 was 90 - 350 m (54 craters) and, for Zone 5, 300 - 2000 m (247 craters). Resultant crater retention ages for Zone 1 and Zone 5 are, respectively, 150 ± 20 Ma and 1.6 ± 0.1 Ga (Appendix 3, Fig A2).This is probably a very approximateLVF age: the few larger craters (or traces of craters) on the LVF might follow an older isochron,on the order of 1-1.5 Ga, which couldbetter represent the LVF formation age, rather than its modification age.With such small numbers (2-3 craters), though, this is a very tentative conclusion. The Zone 5 crater retention age, although complicated by the small number of craters > 2 km, points to basin filling inthe Amazonian. This is later than envisagedby Tanaka et al. (2014) butnot inconsistent with their interpretation of the fill as volcanic.

4. Interpretation

The LVF (Fig. 2) comprises a complex of lobesdescending from the valley sides towards its hypsometric axis, which marks the front between opposing lobes that are competing to follow the same fall line during longitudinal advection downvalley. There are no individual sources along the valley sides, only scoured chutes descending from the convergent troughs incised into the plateaus overlooking the valley, indicating that the lobes originated on these plateaus, not within the valley.Moreover, the chutes are not hanging valleys but are incised into the valley walls and graded to the surface of the LVF complex. Hence, the valley was only partially filled, and likely not originally cut, by the LVF lobe-complex sourced on the plateaus.

The lobate, lineated morphology of Zone 1, including the presence of ring mold craters (Fig. 3a)indicative of an ice-rich substrate (Kress and Head, 2008), are consistent with the LVF being a topographically-bounded icy body. Moreover, the LVF possesses the following characteristics considered to be diagnostic features of martian mid-latitude glaciers (Souness et al., 2012) and which shed more light on the formation and evolution of the entire system. (1) The LVF is surrounded by topography modified by viscous flow over or around obstacles, best represented by the confluent troughs (Fig. 2) graded to the surface of the main LVF from the adjoining upland along distinct topographic corridors (Bennett, 2003). (2) The LVF is texturally and morphologically distinct from upland summital areas and inter-valleys. (3) It displays foliation indicative of down-slope flow, especially in the form of lobes lineated by narrow ridges and furrows (Fig. 3a). Longitudinal flow lineations have been attributed to lateral compression where topography funnels ice into narrow tongues (Stokes and Clark, 1999) and experiences rapid longitudinal extension (Glasser and Gudmundsson, 2012) in a setting of long-term flow stability(Holt et al., 2013; Glasser et al., 2015), explanations clearly consistent with the context of the LVF here. (4) The LVF is a distinct, narrow flow-form laterally confined by the upland valley sides, and (5) bounded longitudinally by pitted, cross-valley, moraine-like ridges (MLR) in

Zone 2. MLR are indicative of the staged retreat of the LVF terminus by backwasting and marginal stagnation and are, therefore, indicative of dynamic compositional and process thresholds. (6) Throughout its course, the LVF has a viscous 'valley fill' surface.

Fig. 8 here

These six key characteristics (Sounesset at., 2012) are consistent with the LVF being a topographically bounded glacier that was supplied by ice converging from surrounding upland. Hence, it is part of an assemblage of glacial forms between latitudes 30˚ to 60˚ in both hemispheres of Mars (Hubbard et al., 2014).

The straight, parallel-sided form of the valley, especially the narrow, trench-like form of the western branch of the system (Fig. 2), bears a striking resemblance to two trenches that cut through highlands zones well west of the Phlegra Montes(Fig. 9) and which are directly along strike (WNW-ESE). The first, ~230 km distant along strike, is ~60 km long. The second, ~450 km distant along strike, is ~110 km long. Both are about 5 km wide, the first being occupied by LVF, the second by a pitted mantle superimposed by lateral mass wasting lobes.The coherence in strike and scale of these trenches with the valley in Phlegra makes it likely that they all originated as grabens along the same fault system, during regional rifting prior to the formation of the LVF. Hence, the trunk valley occupied by the LVF is probably not a typical LVF context, being part of a very long fault system, expressed intermittently as a graben.

Fig 9here

The cross-valley pitted ridges in Zone 2 are interpreted as recessional moraines that formed after the glacier had retreated from the piedmont. The circular pitted mass in Zone 4b is interpreted as dead-ice producing incipient ice stagnation topography. This, together with the intense pitting of the PTF in Zone 3 and the pattern of PTF disruption in Zone 4a, is evidence that the piedmont trench was formerly fully occupied by ice. The pitting of the piedmont surface, especially the proximal piedmont, is evidence that the piedmont is extensively mantled by degradedice rich material. Hence, it is likely that the PTF is a remnant either of outlet glacial ice from the Zone 1 to 2 upland or of a piedmont LDA. The morphology of the breached bedrock ridge bounding Zone 2, including the cleaving of the originally continuous ridge into opposing headlands by incision of the breach at the lowest point of the ridge, reflect the gravitational focusing of a very narrow line of erosion along the hypsometric axis of the small valley bounded by the headlands. Bedrock breaches like this are not typical of fluvial erosion in the absence of a significant step-change in hydrology, involving either discharge (e.g. lake-bursts), baselevel lowering or cross-valley uplift. Hence, the breach is unlikely to reflect pre-glacial fluvial erosion. However, together with the presence of the sinuous re-entrant valley which appears to carve into the LVF nearly adjacent to the breached ridge, these characteristics are consistent with meltwater erosion sourced from ice immediately upslope of the breached ridge. The absence of channels up-valley of the breached ridgeand the re-entrant valley suggests that the meltwater was englacial, not supraglacial, although shallow supraglacial channels could have been removed by surface modification.The re-entrant does not appear to be a pre-existing fluvial or sapping bedrock channel, for there is no evidence of layering or outcrop in its flanks in its upper reaches, unlike incisions into many of the massifs surrounding the graben. It is therefore unlikely that this is a bedrock channel. However, even werethis re-entrant a bedrock channel, its incision by subglacial meltwater prior to exposure by ice marginal decay could not be precluded. The sinuous axis of the re-entrant valley is evidence of proximal proglacial flow.The pitted, hummocky surface of Zone 3 and the disrupted central tract of Zone 4a are consistent with the degradation of a glacial surface that experienced distal collapse along a well-definedpath close to its terminus. The swaths of convex-up, undulatory forms and longitudinal furrows in Zones 4a and 4b are interpreted as fluvial sediment gravity flows.The convex-up, undulatory forms are fluviatile bars, incised by multiple-channel longitudinal flows (the furrows). The sudden appearance of incised bars and furrows at the terminal edge of the central part of Zone 4a suggests that they originated from sediment-bearing liquid flows sourced in this degrading material. The longitudinally furrowed surfaces extending from the lateral parts of Zone 4a into Zone 4b suggests that the disrupted central tract of Zone 4a was the main source of liquid flows, but that some may have been sourced from the Zone 3/4a boundary. The darkest surfaces in Zone 4b and 4c probably represent distal fines from these flows.An alternative hypothesis is that these units are distal lavas, originating in the upland or in the Zone 5 basin that were emplaced before occupation by the LVF. It is unlikely that the Zone 4 materials are lavas associated with volcanic filling of the Zone 5 basin because they are uphill of the basin, which is extremely flat. Also, thePTFis not characterised by flow lobes, break-outs or evidence of fluid propagation along interior channels, arguing against emplacement from the west. Although not definitive evidence against lava, the contextual landsystem is so overwhelmingly glacigenic that the overarching interpretation of the PTF in Zones 3 and 4a,as a remnant glacial thermokarst assemblage, including some mantling proglacial glaciofluvial deposits, is robust even if not definitive without groundtruth.In this context, the central pitted mass(Zone 4b)is consistent with being an isolated mass of dead-ice, abandoned either during ice marginal backwasting or LDA decay.The form running transverse (Fig. 6b, X-Y) to the Zone 4c ridge system is possibly an ice margin remnant, although better resolution imagery is needed to make a more confident interpretation. However, in the context of the total landsystem, the sinuous ridges themselves are consistent with a subglacial to proglacial transition due to ice marginal decay in this location.Taken together with the rest of the landsystem, beginning in the upland at an extant but marginally decayed glacier and terminating in the piedmont at an esker-like ridge system,the relative locations and morphological characteristics of all the components of the landsystem (Fig. 8) are mutually consilient and consistent with its interpretation asa complete glacial system that experienced decay involvingat least one phase of melting and significant meltwater production.

The coherence in strike and width between the valley hosting the LVF and PTFand the two grabens further east (Figs 1 and 9) indicate at least a structural control in the path of the system. However, the breached ridge and sinuous re-entrant valley in the pitted terminal zone of the LVF (Zone 2) and the glacial thermokarst and channels on the PTF are evidence of melting associated specifically with the presence of a regionally significant fault line (the faultpersists along strike for 630 km).The interpretation of the LVF and PTF as a complex glacial system reflecting a large degree of geological control and exhibiting evidence of meltwater activity helps to explain the sinuous ridges in Zone 4c, for their sinuous form, dimensions and context are consistent with an interpretation as eskers. The presence of eskers reflects the former extension of the glacial system to the margins of Zone 5, prior to the staged retreat of the system into the upland valley.

Relatively small eskers, on the scale of the Phlegra ridges, form on Earth at the terminus of glaciers when surface meltwater penetrates to the bed through moulins and crevasses (Boulton et al., 2001). It is possible that the channels in Zone 4 played a role in this respect, ashydraulic coupling between the glacier surface and base is known to amplify basal hydrostatic pressure and generate water-filled basal cavities (e.g. Boulton et al., 2001). In Phlegra, however, geothermal undermelt could have enhanced cavity production through roof melting as a consequence of basal meltwater production.

The continuous but diverging-converging, sinuous form and scale (10^1 m-wide, 10^3 m-long, over an area 4.5 km by 1.25 km) of the Zone 4c ridges are analogous to many small-scale esker complexes on Earth, both recent (e.g. in Spitsbergen, Fig. 10a) and Pleistocene (e.g. the Knockbarron esker in Ireland, Fig. 10b; a complex of closely-spaced, 10^1 m-wide, 10^3 m-long sinuous ridges over an area 1.83 km by 0.63 km; and esker-net complexes in Maine, northeast USA, Fig. 10c). Continuous ridge eskers (Warren and Ashley, 1994) are tunnel fill deposits, representing sedimentation along subglacial meltwater tunnels melted upwards into overlying ice (i.e. R-channels) and bounded by a stable ice margin. However, the moderate length and directional coherence but lateral off-setting of the segments composing some of the ridges here are consistent with a more unstable, probably crevassed, ice margin (Warren and Ashley, 1994). The continuity and sinuosity of RpS are consistent with an interpretation as continuous tunnel fill eskers, but the sharp ridge-crests are indicative of a phase of strong melting and rapid lowering of the overlying ice together with its subglacial debris load (Shreve, 1985). The segmented ridge assemblage Rd could be interpreted as remnants of a single esker (Shreve, 1985) or as a sequence of short beads (Warren and Ashley, 1994). If a short-beaded esker, it represents drainage to an aqueous ice margin characterised by short periods of stability but generally rapid retreat (Warren and Ashley, 1994). It is also possible that Rd represents a time-transgressive assemblage of segments originating first in flows along a medialRpN-conduit and then cross-lapped by RpS. If the vertical arrangement of the ridges in the distal zone represent a chronological evolution, RpS is likely to have been the last active ridge in the complex. Caution is required, however, in the absence of sedimentological exposure, in interpreting time and space relationships among these ridges.

Fig. 10here.

Given the absence of eskers elsewhere in the region, and the likelihood that the PTF is the surface expression of an underlying subglacial fault, the eskers probably reflect spatially focused melting due to enhanced heat flux along the fault strike (*cf*.Lysak, 1992; Lysak and Sherman, 2002; Clauser and Villinger, 1990; Schroeder et al., 2014). It is unlikely that icethickness alone could have caused basal melting; maximum upland ice thickness is unlikely to have exceeded 1.5 km (based on the elevation difference between the plateau around Zone 1 and the surface of Zone 4) and was probably much less, judging by the graded chutes confluent with the LVF surface. Combined with very low mean Amazonian atmospheric temperature (Fastook et al., 2012), the resultant maximum excess pressure of ~5 MPa is insufficient for basal pressure melting. Hence, an additional heat fluxwas required for melting on the scale suggested by the presence of both eskers and extensive channels(cf. Fastook et al., 2012).

The orientation, structure and fault features of Phlegra Montes might have a genetic association with the Elysium Volcanic Centre (EVC; Moore, 1985). Consistent with Vaucher et al. (2009), Platz and Michael (2011) found evidence of EVC and associated regional activity (Elysium Planitia and Cerberus Fossae) spanning ~3.4 Ga to only ~1.4 Ma. Hecates Tholus, the closest EVC component to Phlegra Montes, formed ~350 Ma. The filled grabens in and east of Phlegra Montes are coherent in strike with a super-regional set of linear troughs extending across the northern flank of the Elysium Rise, through Galaxias, to Utopia Planitia. Hence, given the longevity of EVC volcanic processes and the scale of their effects, including the possible genetic linkage between the EVC and faulting in Phlegra Montes, the elevation of heatflux along the Phlegra graben system while occupied by a piedmont outlet glacier during the Late Amazonian cannot be precluded.The construction of the main valley glacier in Phlegra by the convergence of several plateau tributaries into apre-existing strike-valley (Zone 1), could reflect enhanced geothermal heat flux along strike and the development of a positive feedback involving increased basal temperature, melting, basal lubrication and flow velocity (cf. Bennett, 2003). Enhanced geothermal heat flux extending from the strike valley and along the PTF could have amplified this positive feedback, with outputs as higher ice velocity and increased advection, surface down-draw and basal meltwater production.

As no evidence has been presented of esker formation analogous to the Phlegra Montes system elsewhere on Mars, although other fault-bounded glacial systems exist (e.g. Levy et al., 2007), it is worth speculating on the factors that could determine esker potential as an epiphenomenon of enhanced geothermal heatflux. For this to occur, a glacier must occupy a fault during a phase, and at a location, characterised by sufficiently elevated heat flux, either associated with fault emplacement (with significant heat propagation lags) or reactivation. In systems like the Rheingraben or the Kenya Rift, enhanced heatflux commonly persists for 10^7 years, with10^6 - 10^7 years required for heat propagation from the Moho to the surface(e.g. Wheildon et al., 1994).

The glacial hydrological system in Phlegra is unlikely to be replicated in regions with no evidence of Late Amazonian volcanism and fault (re)activation coincident with glaciation. Moreover, because enhanced heatflux is highly concentrated but variable along rift axes, consequential meltwater production and esker formation might have occurred only in restricted spatial and temporal contexts within a single bounding fault, even in the Phlegra case. Considering the Dorsa Argentea eskers, perhaps indicative of Noachian-Hesperian warm-based glacial conditions, Fastook et al. (2012) concluded that atmospheric temperatures must reach -75to −50° Cfor significant basal melting to occur in settings characterised by typical geothermal heat fluxes (45-65 mW.m^{-2}). This represents an enormous climate change but still results in cold based glaciers,implyingthat geothermal conditioning is strongly implicated in the production ofmartian eskers.If subglacial water flux generally tends to be low, due to inherently low atmospheric temperatures, subcritical geothermal heat flux and weak melting, the widespread development of R-channels required for esker formation is, most likely, precluded. Only beneath ice experiencing enhanced melting, evidently due to significant atmospheric temperature excursions and/or elevated geothermal heat flux (Fastook et al., 2012), couldsubglacial water flux increase both down-glacier andtowards the glacier bed sufficiently to allow R-channels to form and remain open. Hence, on Mars, the development and survival of R-channels capable of transporting sufficient quantities of both meltwater and sediment required for esker formation might be very rare, reflecting the short time periods and limited locations in which both atmospheric temperatures and geothermal heat flux combine to exceed the required critical threshold. We note that channels, and other evidence of subglacial to proglacial meltwater routing, occur at the Zone 2 margin and on the Zone 4a surface of the Phlegra system. On this basis, observations of channels closely associated with glacial margins elsewhere on Mars should be re-examined as possible evidence of subglacial to proglacial meltwater routing.

Fig 11 here

5. Implications of glacial melting and liquid flows

5.1 Surface flows

Hubbard et al. 2014 concluded that the extremely rare evidence of supraglacial melting on Mars points only to short-lived, unorganized liquid flows and that no evidence exists of pro-glacial fluvial activity. However, Fassett et al (2010) described glaciers that showed evidence of limited surface melting and proglacial drainage in the Amazonian. Consequently, the consensus is that the thermal regimes of extant martian glacier-like forms are cold, although perhaps not always in the past (Hubbard et al., 2011). The Phlegra glacial system (upland and piedmont) is important, therefore, for it shows evidence of ice-contact glaciofluvial breaching of the ridgeand incision of the re-entrant in the terminal zone of the LVF (Zone 2) and suggests that water from Zone 2 was exported to the PTF in Zone 3. The fluvial systems in Zones 4a and 4b probably originated from sediment-bearing liquid flows sourced on the Zone 3 PTF and from the longitudinally furrowed surface extending beyond the disrupted surface in Zone 4a.

5.2 Basal flows

Interpretations of sinuous ridges on Mars as eskers include the implication that extensive, thick wet based glaciation has occurred (e.g. Kargel and Strom, 1991; Banks and Pelletier, 2008; Banks et al., 2009; Head, 2000; Bernhardt et al., 2013). However, because none of these eskers is associated with an intact glacier, very little is known about the possible range of subglacial hydrology associated with martian esker formation. In the Phlegra landsystem, while the morphology and dimensions of the sinuous ridges in Zone 4c are consistent with their interpretation as eskers, the PTF shows the direct evidence of both subglacial and supraglacial flows in the same glacial system, although the supraglacial flows appear to originate from the emergence of englacial flows(e.g. in Zone 4a from probable glacial ice in Zone 3). Similar emergences from englacial channels are common in glaciers in geothermal zones on Earth (e.g. Waltham, 2001), including the development of sub-aerial channels on surfaces exposed due to the thinning and collapse of ice roofs.

Generally, the presence of eskers implies significant basal routing of meltwater, but not necessarily the production of meltwater at the base. On Earth, subglacial meltwater flows often reflect hydraulic coupling between the glacial surface and the base. Englacial to subglacial conduits that develop within hydraulically coupled systems represent tunnel-confined basal flows of water fed from melting, flows and standing water at the glacier surface (Benn et al., 2012). In Phlegra, however, it is likely that the eskers and surface channels carved by emergent englacial flows reflect conductance of geothermal heat from the subglacial graben through the ice and, therefore, that the formation of the eskers involved both basal production and routing of meltwater. The cessation of excess heat flux from the graben and, therefore, transition of the overlying glacier to a cold based thermal regime in equilibrium with prevailing climate, probably explains the survival of the system, in company with the surrounding glaciers. It should be noted, though, that even on Earth, eskers can be preserved as glacial retreat strands them in an evolving proglacial outwash system (e.g., Fig. 10a).

6. Conclusions

The assemblage of landforms described here is consilient in relief, relative topography and morphology with an interpretation as a wet-based glacial system (Figs 8 and 11). This system presents what appears to be the first identification of martian eskers that can be directly linked to their parent glacier. The observations demonstrate the presence of a wet-based system, implying that, where there is sufficient heat, glaciers on Mars will attain warm/wet based regimes. However, here the energy required for melting came from bottom-up geothermal heating, rather than being due to changes in climate. In the absence of such geological conditioning, glaciers on Mars seem largely incapable of achieving these regimes, overarching climatic control producing only cold based glaciers.Regarding the Phlegra Montes landsystem, it remains to be definitively established if the graben was thermally active during the glacial period, or simply a pre-existing topographic corridor or sink. If it was active, could glacial fast-flowhave been triggered along the geothermal-topographic corridor, enhanced geothermal heating creating a positive feedback involving melting and glacio-dynamics that led to the formation of this possibly unique system?Resolving these problems and effectively contextualising the answerswill require searching elsewhere on Marsfor evidence of geothermal influences on lowland glaciers, including supraglacial melting and proglacial discharges,in the absence of direct observations of eskers.

Acknowledgments

The authors thank Jack Holt and Eric Petersen of the University of Texas, USA, for their help in attempting to de-clutter SHARAD imaging data, and for considering an early draft of this paper.Thanks also to Joe Levy and an anonymous reviewer for their extremely helpful reviews. We thank Peter Fawdon and Laura Brooker at Open University, UK, for helpful insights into an earlier version of the paper and Woody Thompson, Maine Geological Survey, for providing the LIDAR image. MRB was supported by grants from the UK Science and Technology Facilities Council (STFC; grant # ST/L000776/1), the Leverhulme Trust (grant # RPG 397), and the UK Space Agency (grant # ST/L00643X/1).

REFERENCES

Banks, M. E. and Pelletier, J. D. (2008).Forward modeling of ice topography on Mars to infer basal shear stress conditions, *J. Geophys.Res*., 113, E1, http://dx.doi.org/10.1029/2007JE002895.

Banks, M. E., N. P. Lang, J. S. Kargel, A. S. McEwen, V. R. Baker, J. A. Grant, J. D. Pelletier, and R. G. Strom (2009), An analysis of sinuous ridges in the southern Argyre Planitia, Mars using HiRISE and CTX images and MOLA data, *J. Geophys. Res*., 114, E09003, doi:10.1029/2008JE003244.

Benn, D.I., Bolch, T, Hands, K., Gulley, J., Luckman, A., Nicholson, L.I., Quincey, D., Thompson, S., Toumi, R. and Wiseman, S. (2012) Response of debris-covered glaciers in the Mount Everest region to recent warming, and implications for outburst flood hazards, *Earth-Science Reviews*, 114, 156–174.

Benn, D., Gulley, J., Luckman, A., Adamek, A. and Glowacki, P.S. (2009). Englacial drainage systems formed by hydrologically driven crevasse propagation, *Journal of Glaciology*, 55, 191

Bennett, M.R. (2003). Ice streams as the arteries of an ice sheet: their mechanics, stability and significance, *Earth-ScienceReviews*, 61, 309 – 339. doi:10.1016/S0012-8252(02)00130-7.

Bernhardt, H., Hiesinger, H., Reiss, D., Ivanov, M., and Erkeling, G. (2013).Putative eskers and new insights into glacio-fluvial depositional settings in southern Argyre Planitia, Mars, *Planet. Space Sci.*, 85, 261–278.

Boulton, G.S., Dongelmans, P., Punkari, M. and Broadgate, M. (2001). Palaeoglaciology of an ice sheet through a glacial cycle: the European ice sheet through the Weichselian, *Quaternary Science Reviews*, 20, 591-625.

Boulton, G. (2010). Drainage pathways beneath ice sheets and their implications for ice sheet form and flow: the example of the British Ice Sheet during the Last Glacial Maximum, *J. Quaternary Sci*., 25, 483–500.

Clauser, C. and H. Villinger, H. (1990). Analysis of conductive and convective heat transfer in a sedimentary basin, demonstrated for the Rheingraben, *Geophys. J. Int.*, 100, 393-414.

Dickson, J.L., Head, J.W., Marchant, D.R. (2010). Kilometer-thick ice accumulation and glaciation in the northern mid-latitudes of Mars: Evidence for crater-filling events in the Late Amazonian at the Phlegra Montes, *Earth and Planetary Science Letters*, 294, 332–342.

Fassett, C.I., Dickson, J.L., Head, J.W., Levy, J.S and Marchant, D.R. (2010).Supraglacial and proglacial valleys on Amazonian Mars, *Icarus*, 208, 86–100.

Fassett, C. I., Levy, J.S., Dickson, J.L. and Head, J.W. (2014). An extended period of episodic northern mid-latitude glaciation on Mars during the Middle to Late Amazonian: Implications for long-term obliquity history, *Geology*, 42 (9), 763–766, doi: 10.1130/G35798.1.

Fastook, J.L., Head, J.W., Marchant, D.R., Forget, F., Madeleine, J.-B. (2012). Early Mars climate near the Noachian-Hesperian boundary: Independent evidence for cold conditions from basal melting of the south polar ice sheet (Dorsa Argentea Formation) and implications for valley network formation. *Icarus*, 219, 25–40. doi:10.1016/j.icarus.2012.02.013.

Fastook, J.L., Head, J.W. and Marchant, D.R. (2014). Formation of lobate debris aprons on Mars: Assessment of regional ice sheet collapse and debris-cover armoring, *Icarus*, 228, 54–63.

Glasser, N.F. and Gudmundsson, G.H. (2012). Longitudinal surface structures (flowstripes) on Antarctic glaciers, The Cryosphere, 6, 383–391, 2012 www.the-cryosphere.net/6/383/2012/ doi:10.5194/tc-6-383-2012.

Glasser, N.F. Jennings, S.J.A., Hambrey, M.J. and Hubbard, B. (2015).Origin and dynamic significance of longitudinal structures (“flow stripes”) in the Antarctic Ice Sheet, *Earth Surf.Dynam*., 3, 239–249, www.earth-surf-dynam.net/3/239/2015/ doi:10.5194/esurf-3-239-2015.

Hartmann, W. K., and G. Neukum (2001), Cratering Chronology and the Evolution of Mars, Space Sci Rev, 96(1-4), 165–194.

Head, J. W. (2000). Tests for ancient polar deposits on Mars: Origin of esker-like sinuous ridges (Dorsa Argentea) using MOLA data, *Lunar and Planetary Science Conference*, XXXI, Abstract 1116.

Holt, J.W., Safaeinili, A., Plaut, J.J., Head, J.W., Phillips, R.J., Seu, R., Kempf, S.D., Choudhary, P., Young, D.A., Putzig, N.E., Biccari, D. and Gim, Y. (2008). Radar Sounding Evidence for Buried Glaciers in the Southern Mid-Latitudes of Mars, *Science*, 322, 1235 – 1238, doi:10.1126/science.1164246.

Holt, T.O., Glasser, N.F., Quincey, D.J. and Siegfried, M.R. (2013). Speedup and fracturing of George VI Ice Shelf, Antarctic Peninsula*, The Cryosphere*, 7, 797–816, 2013 www.the-cryosphere.net/7/797/2013/ doi:10.5194/tc-7-797-2013).

Hubbard, B. and Nienow, P. (1997).Alpine subglacial hydrology,*Quaternary Science Reviews* 16(9), 939-955.

Hubbard, B., Milliken, R.E., Kargel, J.S., Limaye, A., Souness, C. (2011).Geomorphological characterization and interpretation of a mid-latitudeglacier-like form: Hellas Planitia, Mars, *Icarus*, 211, 330–346.

Hubbard, B., Souness, C. and Brough, S. (2014). Glacier-like forms on Mars, *The Cryosphere*, 8, 2047–2061, www.the-cryosphere.net/8/2047/2014/, doi:10.5194/tc-8-2047-2014.

Ivanov, B. A. (2001), Mars/Moon Cratering Rate Ratio Estimates, in *Chronology and Evolution of Mars*, vol. 12, edited by R. Kallenbach, J. Geiss, and W. K. Hartmann, pp. 87–104, Springer Netherlands, Dordrecht.

Kargel, J.S. and Strom, R.G. (1991). Terrestrial glacial eskers: analogs for martian sinuous ridges, *Lunar and Planetary Science Conference*, XXII, 683-684.

Kochel, R.C. and Peake, R.T. (1984). Quantification of waste morphology in Martianfretted terrain. In: Proc. Lunar Sci. Conf. 15. *J. Geophys. Res*. Suppl. 89, C336–C350.

Kneissl, T., S. van Gasselt, and G. Neukum (2011), Map-projection-independent crater size-frequency determination in GIS environments—New software tool for ArcGIS, *Planet. Space Sci.*, *59*(11-12), 1243–1254, doi:10.1016/j.pss.2010.03.015.

Kress, A.M. and Head, J.W. (2008). Ring-mold craters in lineated valley fill and lobatedebris aprons on Mars: evidence for subsurface glacial ice, *Geophys. Res. Lett.*, 35 (23), L23206, http://dx.doi.org/10.1029/2008GL035501.

Kress, A., Head, J.W., Safaeinili, A., Holt, J., Plaut, J., Posiolova,L., Phillips, R., Seu, R. and the SHARAD team (2010). Age and stratigraphic relationships in massif-debris-apron terrain in western Phlegra Montes, Mars, *41st Lunar and Planetary Science Conference*, Abstract 1166.

Levy, J.S., Head, J.W., Marchant, D.R., 2007. Lineated valley fill and lobate debris apron stratigraphy in Nilosyrtis Mensae, Mars: Evidence for phases of glacial modification of the dichotomy boundary, *Journal of Geophysical Research:Earth Surface*, 112, doi:10.1029–2006JE002852. doi:10.1029/2006JE002852.

Lysak S. (1992). Heat flow variations in continental rifts, *Tectonophysics*, 208, 309-323.

Lysak, S.V. and Sherman, S.I. (2002). Terrestrial heat flow in areas of dynamic influence of faults in the Baikal rift zone, *EGU Stephan Mueller Special Publication Series*, 2, 153–160.

Malin, M.C., Bell, J.F., Cantor, B.A., Caplinger, M.A., Calvin, W.M., Clancy, R.T., Edgett, K.S., Edwards, L., Haberle, R.M., James, P.B., Lee, S.W., Ravine, M.A., Thomas, P.C. and Wolff, M.J. (2007). Context Camera Investigation on board the Mars Reconnaissance Orbiter, *J. Geophys. Res*., 112, E5, http://dx.doi.org/10.1029/2006JE002808.

Michael, G.G. and Neukum, G. (2010). Planetary surface dating from crater size–frequency distribution measurements: Partial resurfacing events andstatistical age uncertainty. *Earth Planet. Sci. Lett*., 294, 223–229. doi:10.1016/j.epsl.2009.12.041.

Milliken, R. E., Mustard, J.F, and Goldsby, D.L. (2003). Viscous flow features on the surface of Mars: Observations from high resolution Mars Orbiter Camera (MOC) images, *J.Geophys. Res.*, 108(E6), 5057, doi:10.1029/2002JE002005.

Moore, J.M. (1985). The origin of the Phlegra Montes, Mars, Lunar and Planetary Science XVI, 573-574, Abstract 16_573M.

Morgan, G.A., Head, J.W. III and Marchant, D.R. (2009)Lineated valley fill (LVF) and lobate debris aprons (LDA) in the Deuteronilus Mensae northern dichotomy boundary region, Mars: Constraints on the extent, age and episodicity of Amazonian glacial events, *Icarus*, 202, 22-38.

Neukum, G. and Jaumann, R. (2004). HRSC: The High Resolution Stereo Camera of Mars Express. In *Mars Express: The Scientific Payload*, edited by A. Wilson, 17–35. Noordwiijk: ESA Publications Division.

Parsons, R.A., Nimmo, F. and Miyamoto, H. (2011). Constraints on martian lobate debris apron evolution and rheology from numerical modeling of ice flow, *Icarus*, 214, 246–257.

Platz, T. and Michael, G. (2011).Eruption history of the Elysium Volcanic Centre, Mars, Geophysical Research Abstracts, 13, EGU2011-13166, 2011.

Safaeinili, A., Holt, J., Plaut, J., Posiolova, L., Phillips, R., Head, J.W., Seu, R. and the SHARAD team (2009). New radar evidence for glaciers in Mars Phlegra Montes region, *40th Lunar and Planetary Science Conference*, Abstract 1988.

Schroeder, D.M., Blankenship, D.D., Young, D.A. and Quartini, E. (2014).Evidence for elevated and spatially variable geothermal flux beneath the West Antarctic Ice Sheet, *Proceedings of the National Academy of Sciences*, 111, 25, 9070-9072.

Seu, R., Phillips, R.J., Biccari, D., Orosei, R., Masdea, A., Picardi, G., Safaeinili, A., Campbell, B.A., Plaut, J.J., Marinangeli, L., Smrekar, S.E. and Nunes, D.C., (2007). SHARAD sounding radar on the Mars Reconnaissance Orbiter, *J. Geophys. Res*., 112, E5, http://dx.doi.org/10.1029/2006JE002745

Shreve, R.L. (1985). Esker Characteristics in terms of glacier physics, Katahdin esker system, Maine, *Geological Society of America Bulletin*, 96, 639–646, doi: 10.1130/ 0016-7606(1985)962.0.CO;2.

Souness, C., Hubbard, B., Milliken, R.E. and Quincey, D. (2012). An inventory and population-scale analysis of martian glacier-like forms, *Icarus*, 217, 243–255.

Squyres, S W. (1979). The distribution of lobate debris aprons and similar flows on Mars.*J.Geophys. Res.*, 84, 8087-8096.

Stokes, C.R. andClark, C.D.(1999). Geomorphological criteria for identifying Pleistocene ice streams.*Annals of Glaciology*, 28(1), 67- 74, doi:10.3189/172756499781821625.

Tanaka, K.L., Skinner, J.A., Dohm, J., Irwin, R.P., III, Kolb, E.J., Fortezzo, C.M., Platz, T., Michael, G.G., Hare, T.M., 2014. Geologic map of Mars: U.S. Geological Survey Scientific Investigation Maps, Map 3292.

Thompson, W. B. (2014). Maine's Eskers, Maine Geological Survey Website, Geological Site of the Month, January 2014.http://www.maine.gov/dacf/mgs/explore/surficial/sites/jan14.pdf, accessed on 23 April 2015.

Vaucher, J., Baratoux, D., Toplis, M.J., Pinet, P., Mangold, N., Kurita, K. (2009). The morphologies of volcanic landforms at Central Elysium Planitia: Evidence for recent and fluid lavas on Mars, *Icarus* 200, 39–51.

Waltham, T. (2001). Guide to the volcanoes of southern Kamchatka, Russia, *Proceedings of the Geologists' Association*, 112, 67-78.

Warner, N.H., Gupta, S., Calef, F., Grindrod, P, Boll, N., and Goddard, K. (2015). Minimum effective area for high resolution crater counting of martian terrains. *Icarus*, 245, 198-240, doi:10.1016/j.icarus.2014.09.024

Warren, W.P. and Ashley, G.M. (1994). Origins of the ice-contact stratified ridges (eskers) of Ireland, *J. Sedimentary Research*, A64, 433-449.

Wheildon, J., Morgan, P., Williamson, K.H., Evans, T.R. and Swanberg, C.A. (1994). Heat flow in the Kenya rift zone, *Tectonophysics*, 236, 1–4, 131-149, doi:10.1016/0040-1951(94)90173-2.

Zuber, M.T., Smith, D.E., Solomon, S.C., Muhleman, D.O., Head, J.W., Garvin, J.B., Abshire, J.B. and Bufton, J.L. (1992).The Mars Observer Laser Altimeter Investigation,*J. Geophys. Res.*, 97, 7781–97.

Figure captions

Figure 1.Location of southern Phlegra Montes. Background image is THEMIS daytime mosaic overlain by colourised MOLA topography data (purple is low elevation, brown is high). Inset shows position of this figure in relation to a global MOLA hillshade map of Mars. Locations of other figures shown by white boxes.Image credit NASA/JPL/ASU/MOLA science team.

Figure 2. Southern Phlegra study region. a) 6m/pixel CTX mosaic of the study region. The different zones in the system are marked, as are the inferred flow directions of the lineated valley fill (LVF) occupying the east-west trending valley. b) Colourised topography (MOLA data overlain on CTX mosaic) information for the study region. Position of topographic profile (bottom panel) shown by heavy black line. Note the LVF summital region and western piedmont upland, the steep convex transition from zone 2 to 3, and the gentle slopes in zones 3-5. Image credits NASA/JPL/MSSS/MOLA science team. North is up in this and all other images unless stated otherwise.

Figure 3.LVF morphology and confluent chutes. a) Zone 1 morphology. The valley is occupied by the LVF feature. Lobate forms are picked out in white. Note also the longitudinal lineations, ring-mold impact craters (e.g., black arrow) and one fresh impact crater (white arrow). The pitted region marking the start of zone 2 is seen at the right of the image. b) Confluent valleys and chutes on the northern valley wall (arrowed). The floors of these valleys have textures similar to that seen on the LVF, and are clearly indicative of headward erosion orthogonal to

the main valley trend. Note that the valleys floors are topographically above the surface of the main valley LVF but connected with it via graded chutes. Image credits NASA/JPL/MSSS.

Figure 4.Zones 2 and 3. a) The thinning fill of Zone 2 is dominated by two cross-valley bands of hectometer-scale pits (labelled and arrowed) enclosed by an arcuate bedrock ridge, breached at its hypsometric axis (Q) between two headlands (A and B). The pitted fill enclosed by the ridge is indented by a narrow valley (P) and the LVF is incised by a re-entrant valley (X) that cuts through the southern limb of the bedrock ridge (south of B) and terminates in a complex of large hummocks (Y). (b) Zone 3 (the proximal piedmont) is dominated by the pitted piedmont trench fill (PTF) confined by steep lateral edges, rising up to 100 m above the fill. Extending for ~2.5 km from the ridge-breach in Zone 2 is a sinuous, thread-like crease (black arrows). The edges of the trench in this zone are indented by erosional alcoves (white arrows). Image credits NASA/JPL/MSSS.

Figure 5.Zone 4. a) Zone 4a. Note the central disrupted reach, and the two bounding, subtly-furrowed platforms (FN, north, and FS, south). b) Zone 4b. The northern and southern furrow patterns that begin in zone 4a show more organization in zone 4b. The furrows link to form a continuous, bifurcating channel-like system that is directed to the north and south of a hummocky and pitted central mass. Inferred flow directions are shown by the larger white arrows. Note the darker regions overlying parts of the southern branch and possible infilling of

the northern branch by this dark material – smaller white arrows with '?' – presumably having been transported along the southern branch of the system. Image credits NASA/JPL/MSSS.

Figure 6.Zone 4c.a). Zone 4ccontains a distinctive sinuous ridge system (box shows location of Fig. 6b) within a parabolic embayment that has tiered alcoved margins.. The linked systems of furrows, visible in zone 4a and 4b appear to terminate at the scarp that defines this parabolic embayment. b) Close-up showing details of the sinuous ridges. The pattern has been picked-out in black to show the difference in form between the northern (RpN) and southern (RpS) ridges. The form running transverse (X-Y) to the ridge system is possibly an ice margin remnant.Image credits NASA/JPL/MSSS.

Figure 7.Zone 5. a) Surface textures in Zone 5. Note the rectilinear patterns on the Zone 5 surface, and patterns of what appear to be subtle fractures. Arrow shows ridge system seen in Zone 4c. b) MOLA topographic data for Zone 5. The yellow line shows the morphological boundary of zone 5. The different coloured regions indicate the areas of different elevation in the lowest parts of the region, based on MOLA gridded data. Regions higher than -3240m elevation are left uncoloured. The area characterised by marginal LDAs, in the northern part of the basin, is marked X. The background is a HRSC nadir-looking visible image. Although the basin is > 200 km in length, the variations in depth across it are only about 100m. Image credits NASA/JPL/MSSS/ MOLA science team and ESA/DLR/FUBerlin.

Figure 8. Cartogram derived from CTX imaging data (see online Appendix for image details) depicting the relative locations and major morphological characteristics of the landsystem.

Figure 9. Grabens along strike of the valley in the Phlegra study area. Locations of these figures are given in Fig.1. Image is THEMIS daytime mosaic. Image credits NASA/JPL/ASU.

Figure 10.Terrestrial analogue eskers. a) Esker system in Svalbard. These eskers have been revealed by retreat of the AustreTorellbreen glacier in southwest Svalbard. The glacier itself is just to the north of the image, with the previous glacial advance direction (inferred from lineaments, furrows and moraines) shown by the large white arrow. South of the smaller white arrows, the esker system is well-organised, with clearly defined ridges, similar in morphology to those seen in the Phlegra Montes region on Mars. Image centered at approximately 77.14N, 15.18E. Image credit Norwegian Polar Institute. b) High resolution (0.5 m) aerial photograph of the Knockbarron esker near Kinnitty, County Offaly, Ireland. This esker complex consists of ridges of coarse gravels and sands deposited by subglacial meltwaters flowing locally SW-NE in subglacial tunnels and discharging into a small ice marginal lake (not shown) after the Last Glacial Maximum. Image credit DigitalGlobe.c) High-resolution (2 m) LIDAR shaded-relief image of the Monroe esker network in Maine, USA. This small section of branching, complex ridges (an ‘esker-net’) is part of a larger system (Thompson, 2014) and similar in morphology and

ridge-plan to the martian example described here. North is to the bottom in this image. Image credit Maine Geological Survey.

Fig 11. Oblique view of the entire system, created using a 6 m/pixel CTX mosaic draped over 50 m grid HRSC topographic data. This viewpoint shows the continuity of the system, from upland to distal piedmont, including the eskers. The system is zoned by the prevalence of different landforms but the landforms comprising each zone are consistent with analogue glacial systems on Earth. This view also shows the relative relief of the components of the system, emphasizing both the continuity of the valley-trench lineament and the outflow of the glacier from the upland valley into and through the piedmont trench/graben. The baselevel-like nature of Zone 5 is also clearly expressed.

Eskers in a complete, wet-based glacial system in the Phlegra Montes region, Mars

Colman Gallagher and Matt Balme

Keywords (to be included in main text):
Mars; glacier; eskers; wet base; geothermal control

Highlights

- The first identification of martian eskers directly linked to their parent glacier.
- The Eskers are at the degraded terminus of a graben-confined glacier.
- The eskers are evidence of glacial melting and a wet-based regime.
- Melting was due to enhanced geothermal heat flux, not climate warming.
- These are new insights into glacial behaviour and meltwater production on Mars.

Figure
Click here to download high resolution image

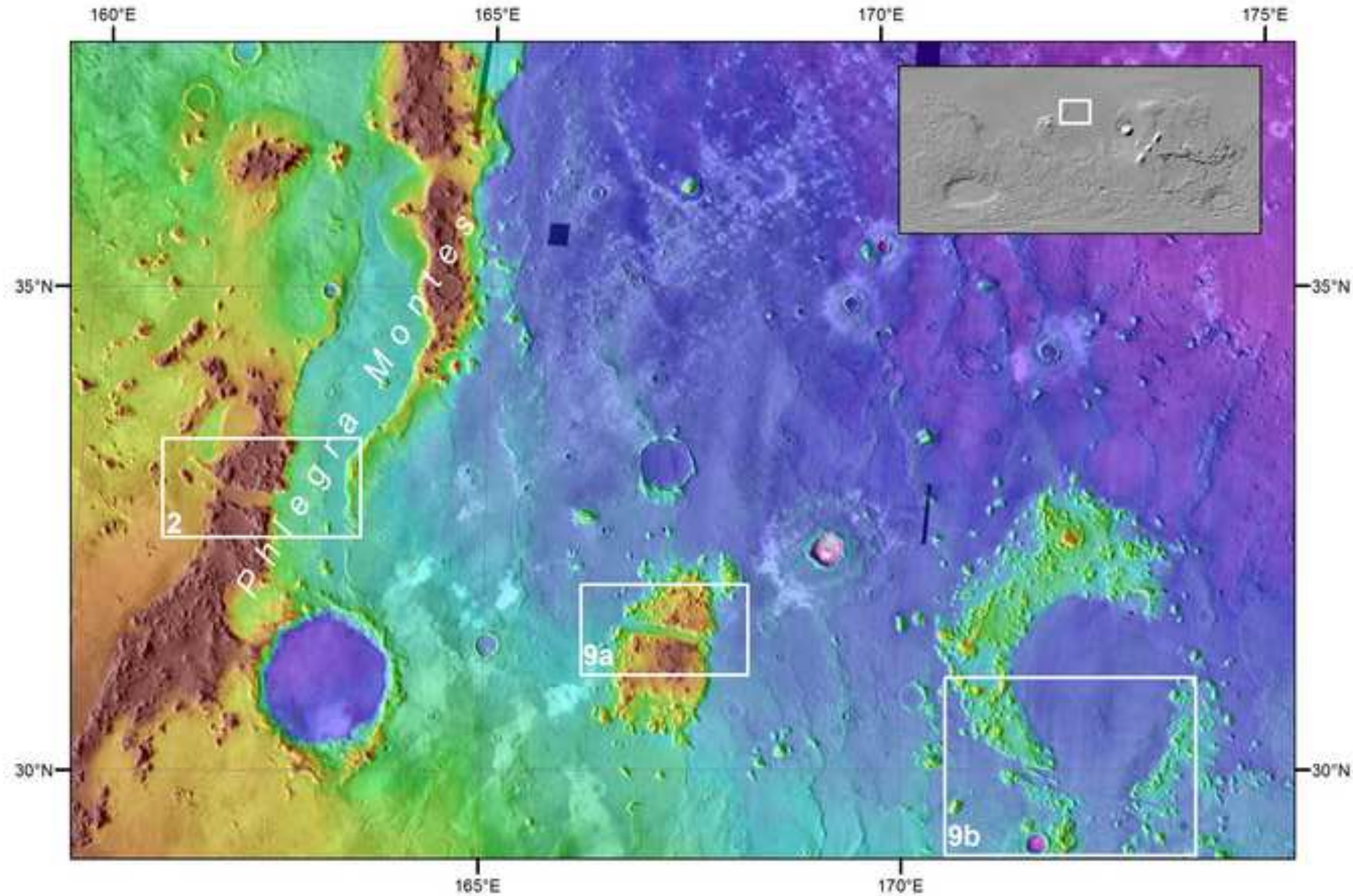

Figure
Click here to download high resolution image

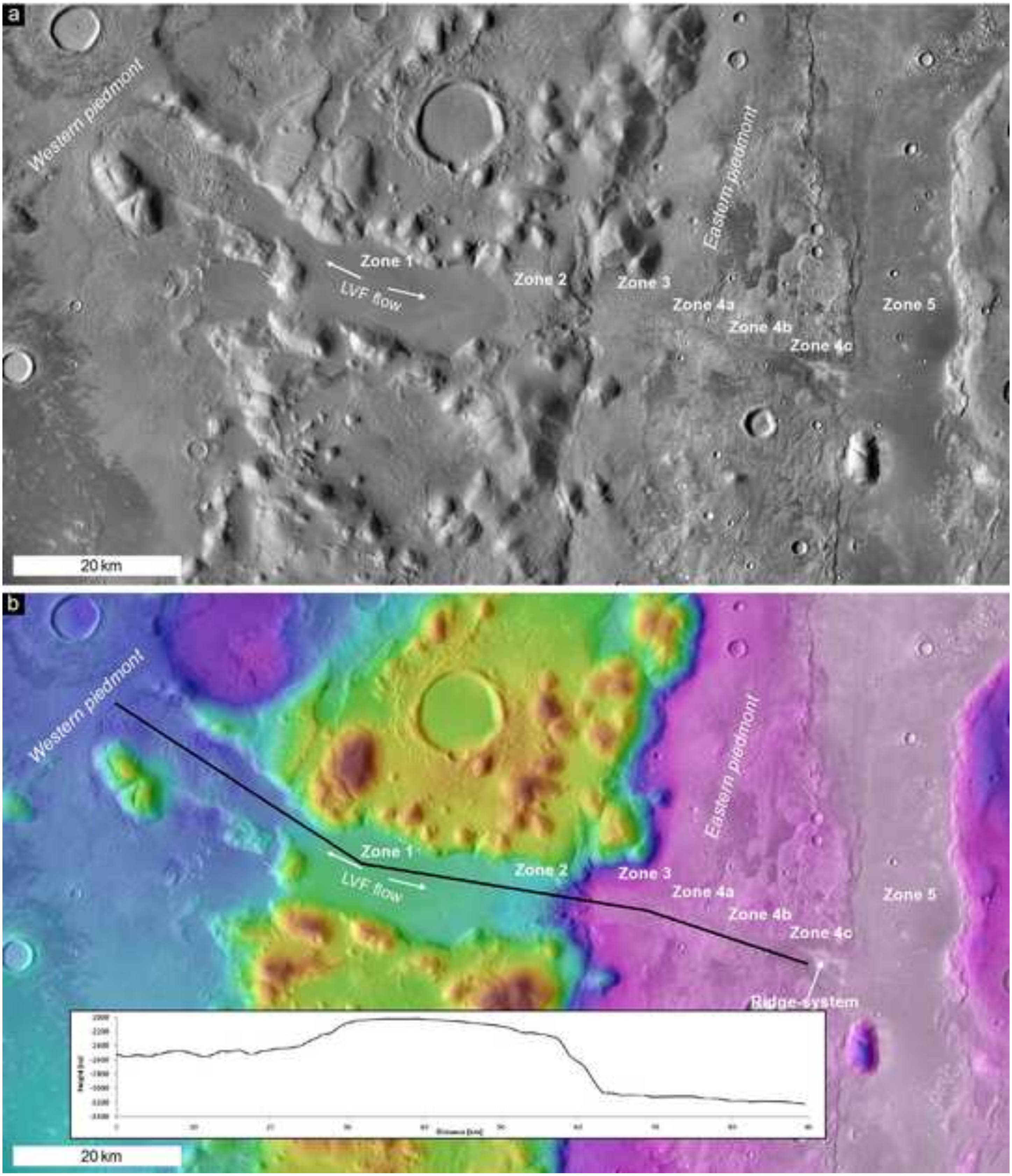

Figure

Click here to download high resolution image

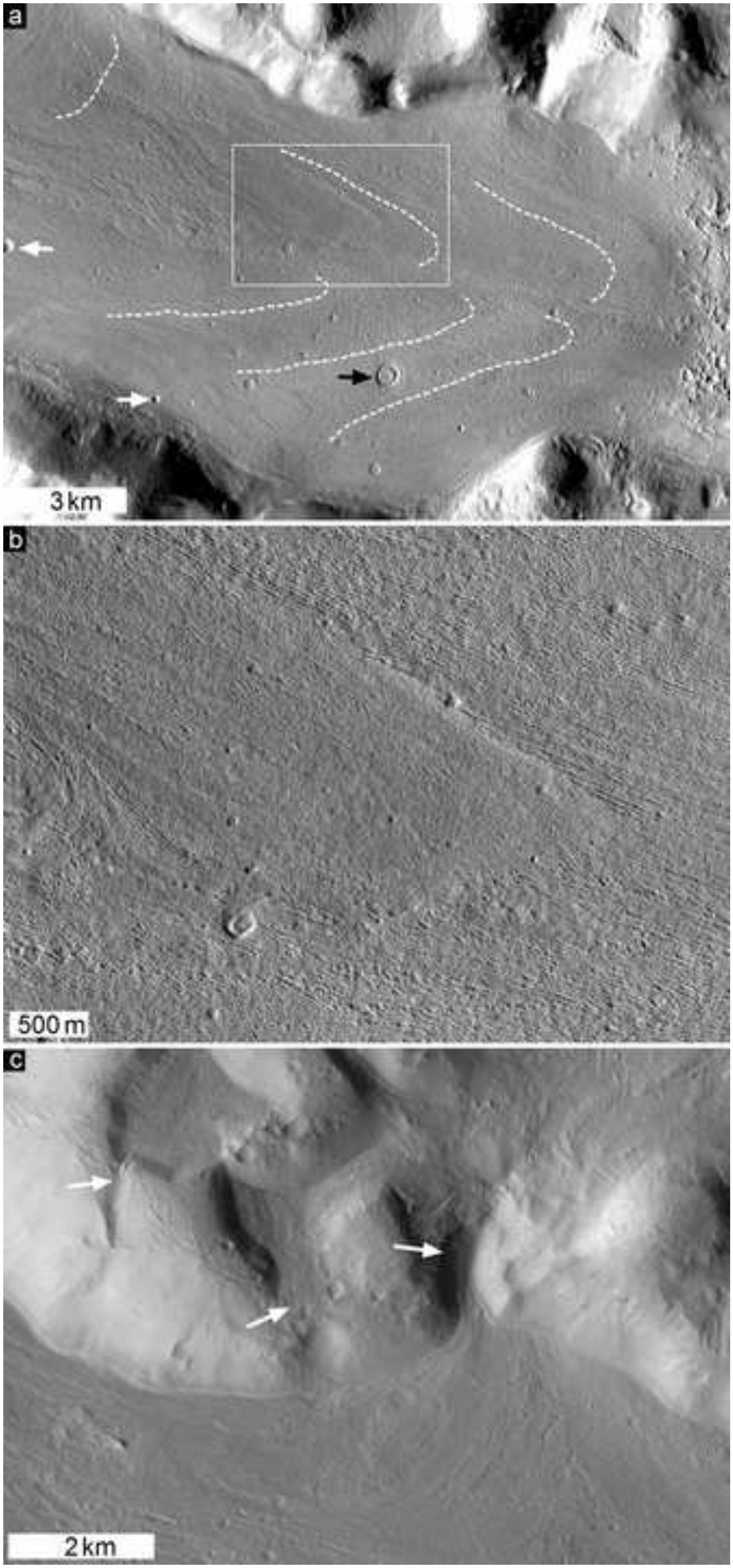

Figure

Click here to download high resolution image

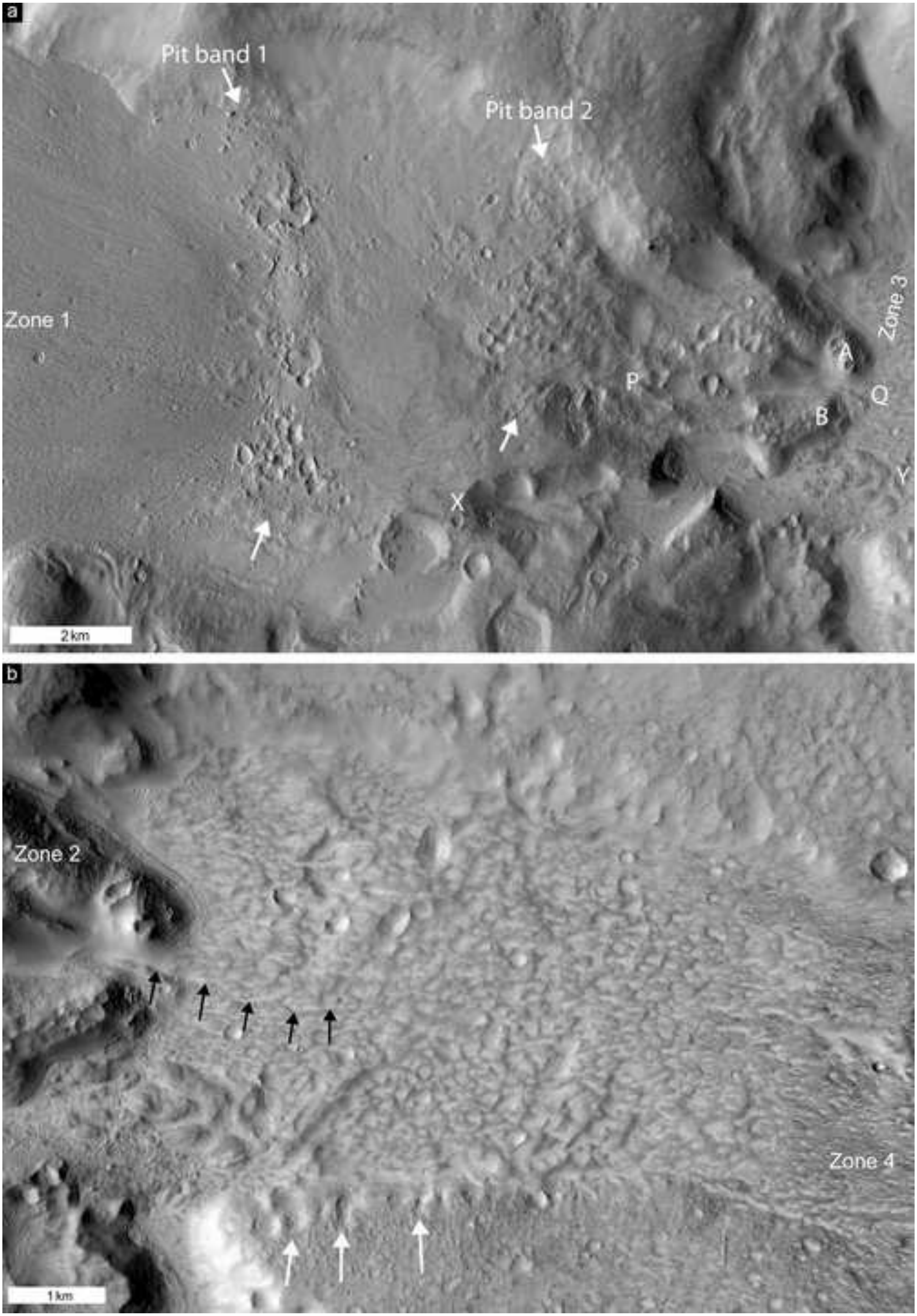

Figure
Click here to download high resolution image

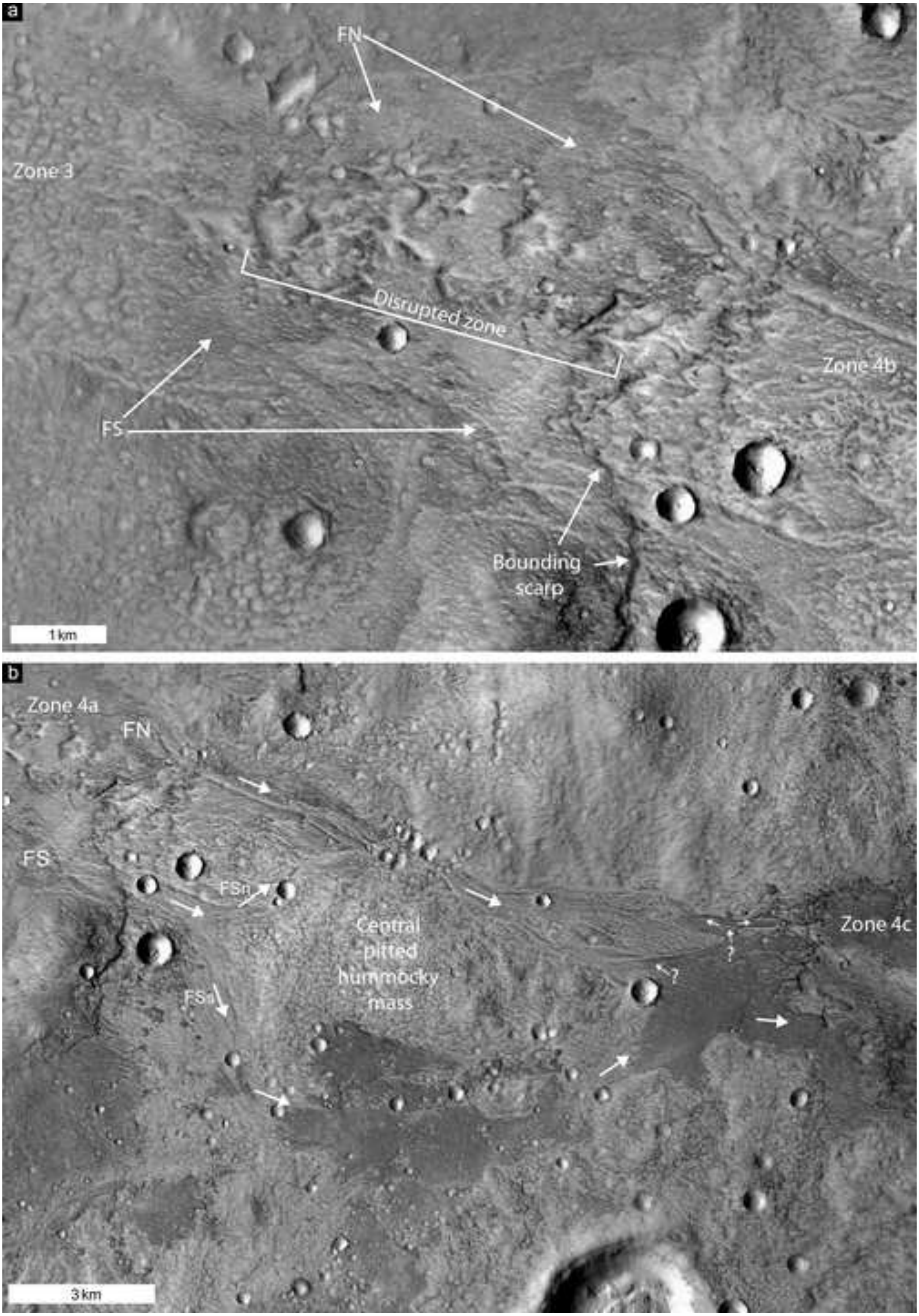

Figure

Click here to download high resolution image

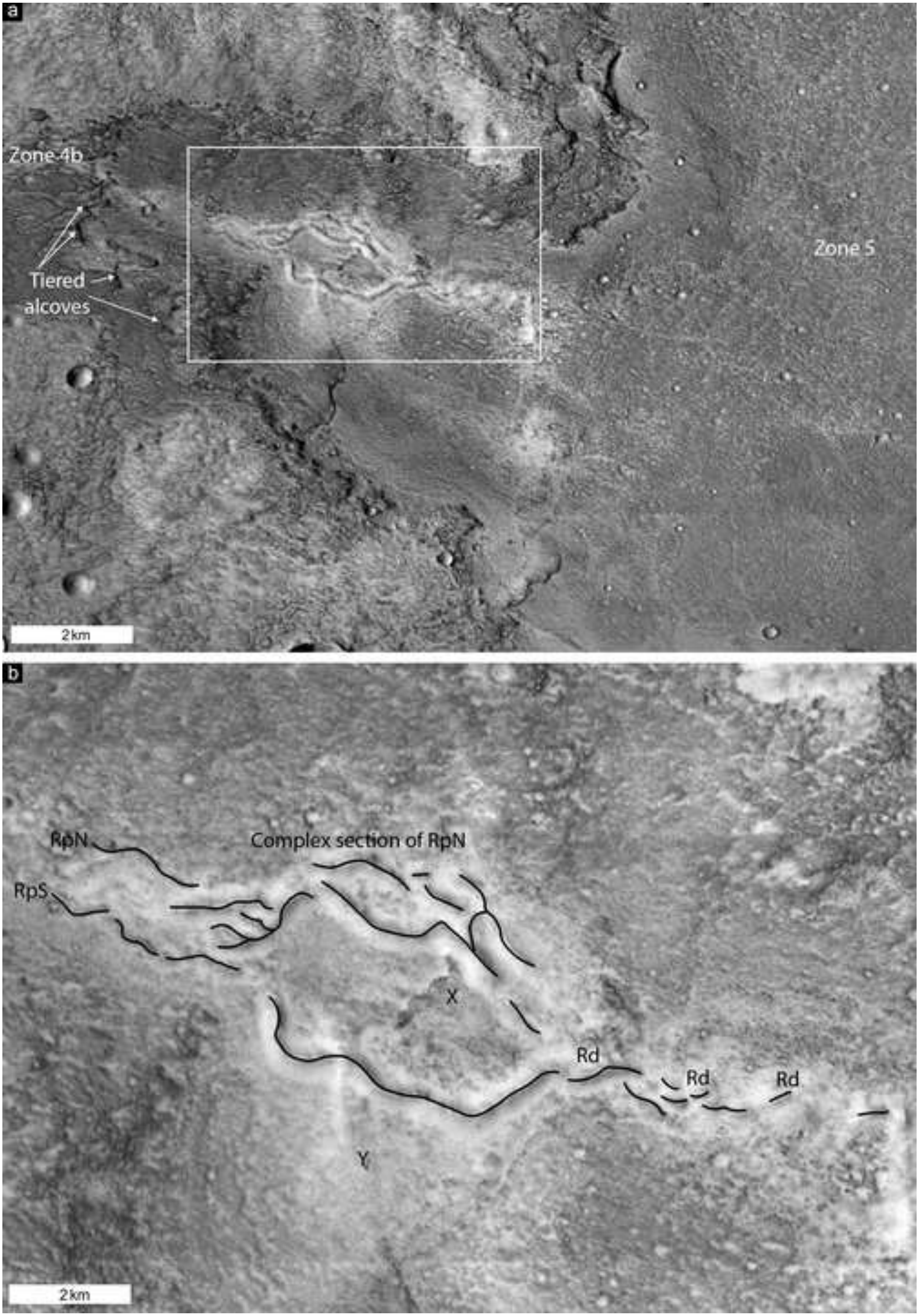

Figure
Click here to download high resolution image

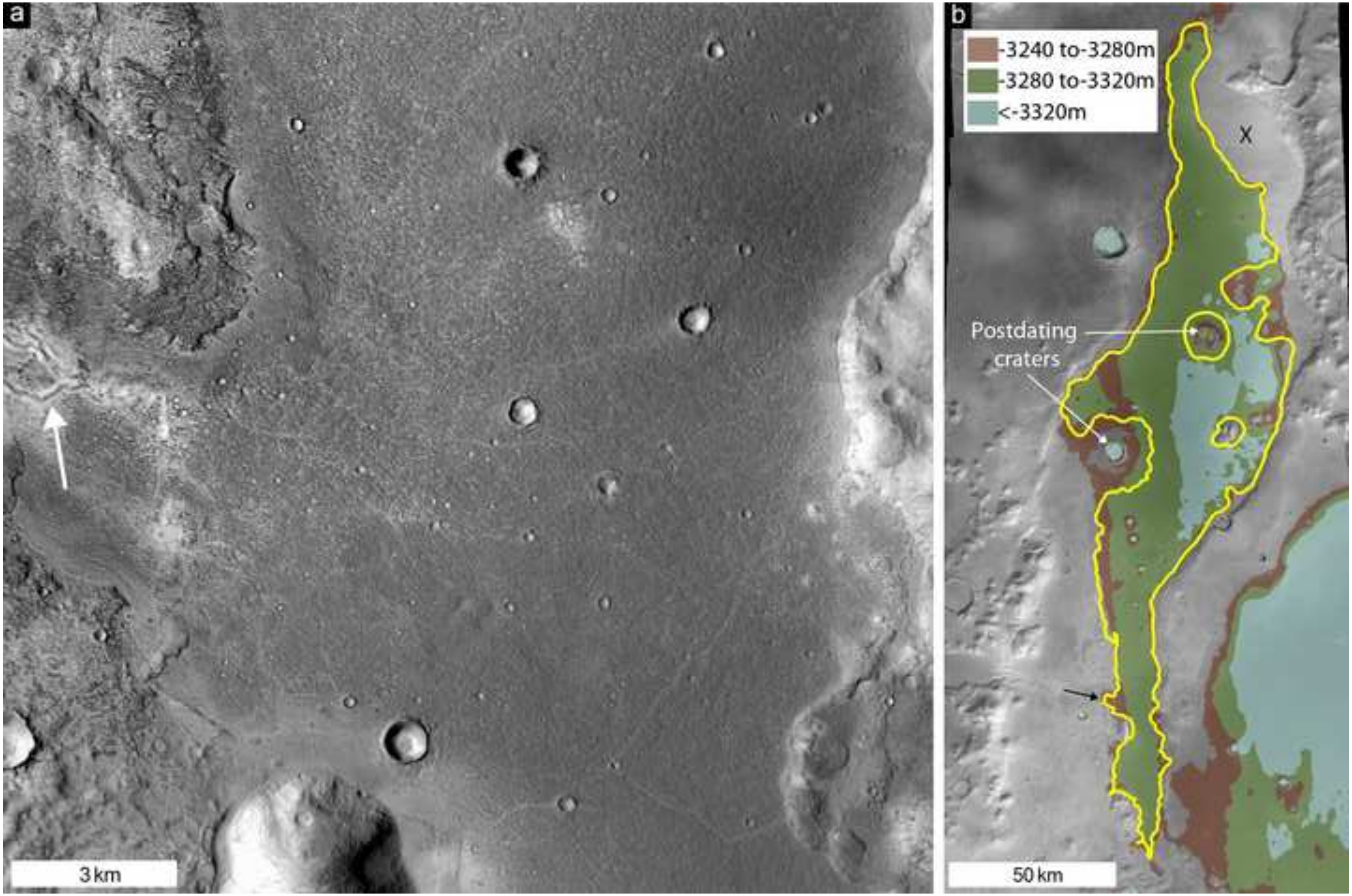

Figure
Click here to download high resolution image

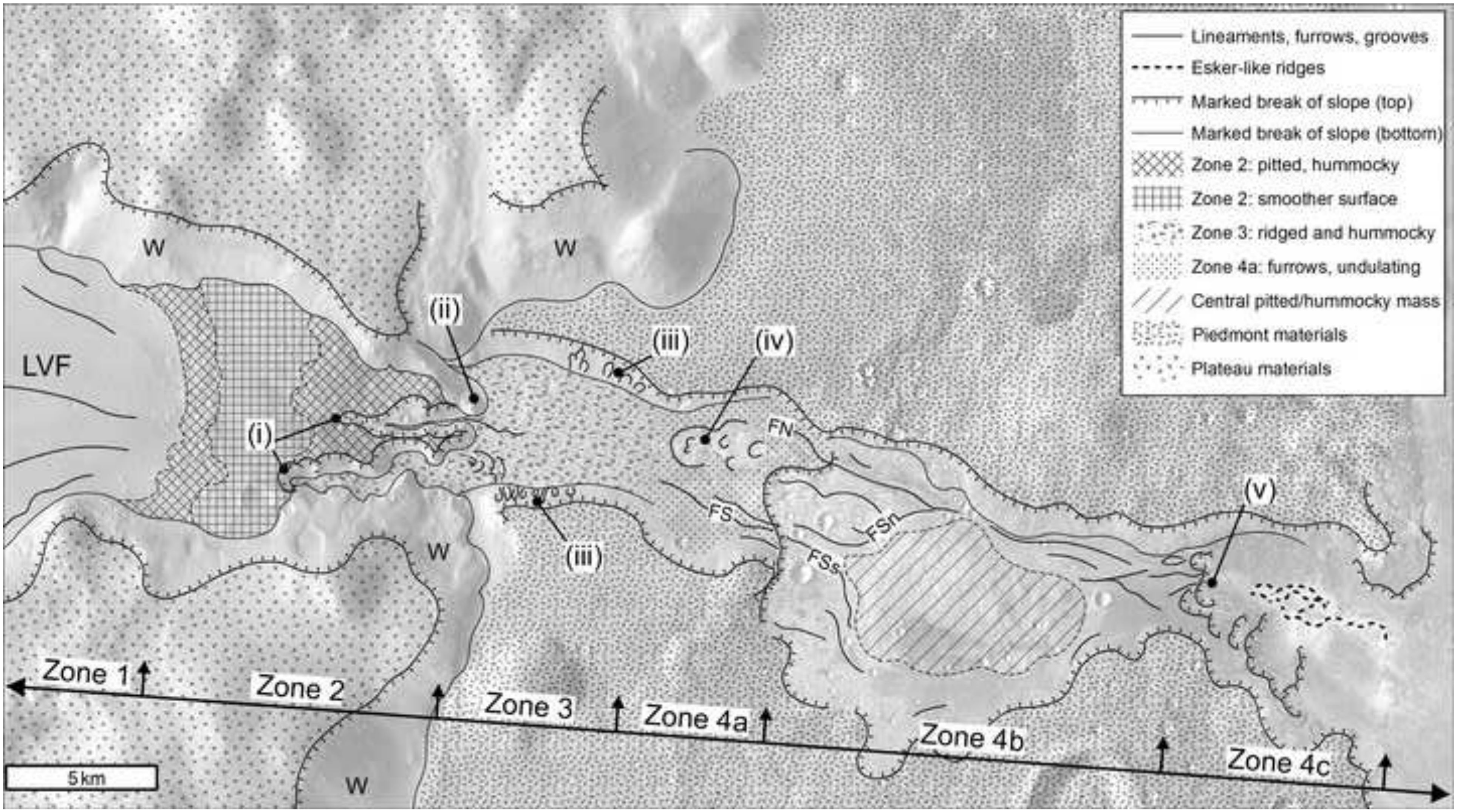

Figure

Click here to download high resolution image

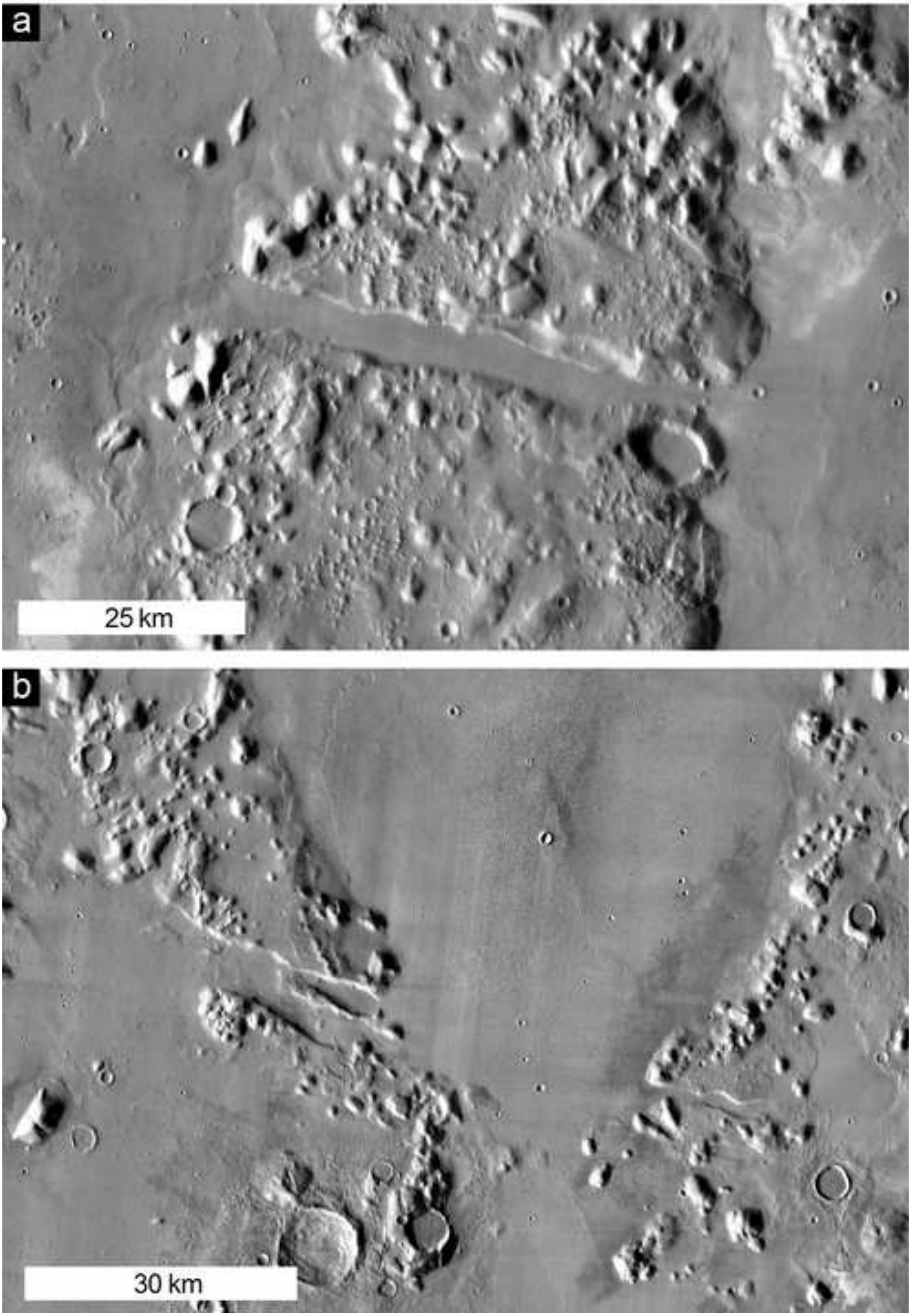

Figure

Click here to download high resolution image

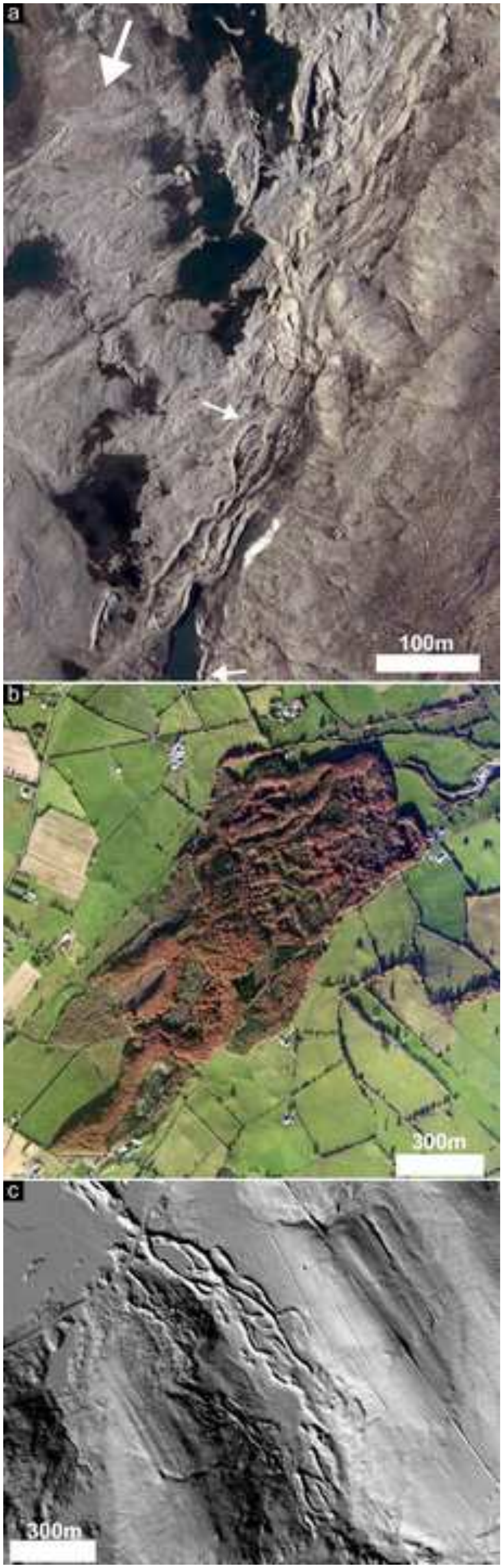

Figure
Click here to download high resolution image

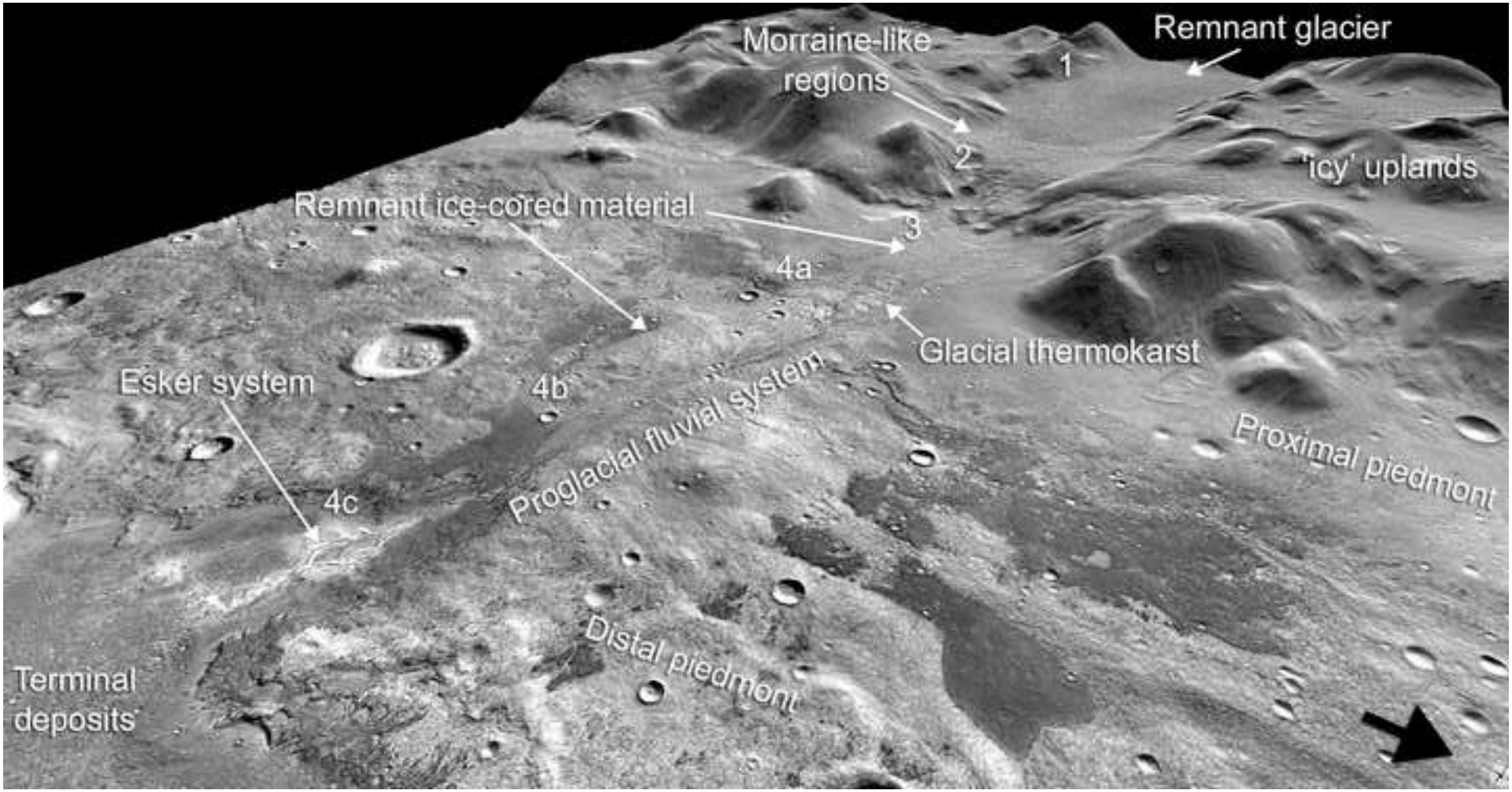

Figure (high-resolution)
Click here to download Figure (high-resolution): CG_phlegra_Fig1_revised.tif

Figure (high-resolution)
Click here to download Figure (high-resolution): CG_phlegra_Fig3_Revised.tif

Figure (high-resolution)
Click here to download Figure (high-resolution): CG_phlegra_Fig5_revised.tif

Figure (high-resolution)
Click here to download Figure (high-resolution): CG_phlegra_Fig6_v2.tif

Figure (high-resolution)
Click here to download Figure (high-resolution): CG_phlegra_Fig7.tif

Figure (high-resolution)
Click here to download Figure (high-resolution): CG_phlegra_Fig8.tif

Figure (high-resolution)
Click here to download Figure (high-resolution): CG_phlegra_Fig9.tif

Figure (high-resolution)
Click here to download Figure (high-resolution): CG_phlegra_Fig11.tif

Figure (high-resolution)
Click here to download Figure (high-resolution): CG_phlegra_Fig4.tif